Biosensors and Bioelectronics 167 (2020) 112457

Contents lists available at ScienceDirect

Biosensors and Bioelectronics

journal homepage: http://www.elsevier.com/locate/bios

Lab in hydrogel portable kit: On-site monitoring of oxalate

Rui Jin [a,1], Lianjing Zhao [a,1], Xu Yan [a,*], Xiaosong Han [b], Mengqi Liu [a], Yue Chen [a], Qingyun Li [a], Dandan Su [a], Fangmeng Liu [a], Peng Sun [a], Xiaomin Liu [a], Chenguang Wang [a], Geyu Lu [a,**]

[a] State Key Laboratory of Integrated Optoelectronics, Jilin Key Laboratory on Advanced Gas Sensor, College of Electronic Science and Engineering, Jilin University, Changchun 130012, People's Republic of China

[b] College of Computer Science and Technology, Jilin University, Changchun, 130012, People's Republic of China

ARTICLE INFO

Keywords:
Oxalate
Target-responsive hydrogels
Oxidase-like activity
Point-of-care detection
Smartphone

ABSTRACT

Oxalate is commonly employed as adjuvant of pesticide agent, causing renal injury of human even in trace residues. Despite the great achievements of the existing point-of-care testing (POCT) technology, accurate on-site screening of oxalate remains a tricky issue. To this aim, we proposed a "lab in a tube" platform which integrated portable hydrogel kit with smartphone for real-time monitoring of oxalate to achieve quantitatively precise analysis. In this work, a stimuli-responsive hydrogel-based kit was constructed via embedding manganese dioxide (MnO_2) nanosheets into sodium alginate hydrogel system. Based on the intrinsic oxidase-like activity, MnO_2 nanosheets-based nanozyme triggered color reaction by introducing a common sensing probe 3,3′,5,5′-tetramethylbenzidine. Meanwhile, the presence of oxalate would decompose MnO_2 nanosheets, inducing the decrease of nanozyme activity, which resulted in the color response of portable kit. Coupling with ImageJ software, the image information of kit captured via smartphone could be transduced into the hue intensity, which provided a directly quantitative tool to detect oxalate with a detection limit of 8.0 μmol L^{-1}. This portable smartphone biosensor was successfully applied for screening urine sample within 10 min for high-throughput analysis (twelve samples) without the need for any advanced analytical instruments. Based on the merits of simple operation, cost-efficiency, and good selectivity, the availability of the miniaturized biosensor platform for POCT will achieve the requirements of routine screening and disease prevention.

1. Introduction

Pesticides are important agricultural production materials, and they are the most effective and irreplaceable intervention methods for the current and future internal restructuring of crop diseases, pests and weeds (Mercey et al., 2012; Yan et al., 2018). The vast majority of pesticide raw materials cannot be directly sprayed with water or otherwise evenly dispersed, covering the object of prevention or its place of activity (Uniyal and Sharma, 2018). Thus, various auxiliary substances (single component or mixture of multiple components) need to be added during the processing and application of pesticide preparation products (He et al., 2019). These pesticide adjuvants are the essential component of pesticide formulation products, which play a significant role in improving the efficacy of pesticide formulations, stabilizing the quality of formulation products, and reducing the active ingredients of pesticides. Oxalate is a commonly used non-surfactant pesticide adjuvants, its excessive use can lead to pesticide adjuvants residues entering the human body. The presence of the excess concentration of oxalate (>300 μmol L^{-1}) in urine indicates a large amount of crystal deposits in the kidneys, which will greatly increase the possibility of urolithiasis (Gan et al., 2019). Certainly, an accurate, rapid and efficient determination of oxalate is of great significance for poisoning assessment. A variety of analytical methods have been investigated to for oxalate determination in urine, food or plasma, such as spectrophotometry (Zhai et al., 2006), enzyme electrode biosensor (Hong et al., 2003), ion chromatography (del Nozal et al., 2000; Maya et al., 2011), and gas chromatography (Li et al., 2008). However, cost-prohibitive, large numbers of samples, and the lack of pocket-sized device or an expert technician limit their on-site analysis. Herein, there is a significant motivation to develop alternative methods for measuring oxalate in

* Corresponding author.
** Corresponding author.
E-mail address: yanx@jlu.edu.cn (X. Yan).
[1] These authors (R. Jin and L.J. Zhao) contributed equally to this work.

https://doi.org/10.1016/j.bios.2020.112457
Received 7 April 2020; Received in revised form 20 June 2020; Accepted 14 July 2020
Available online 9 August 2020

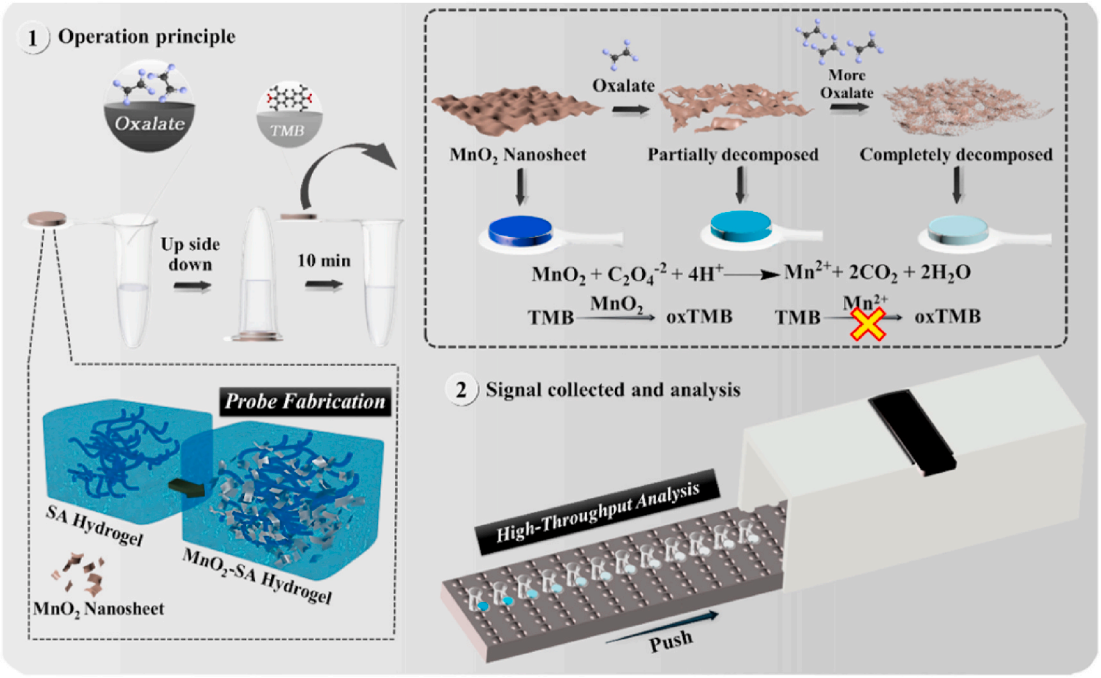

Scheme 1. Schematic illustration of the target-responsive hydrogel platform.

a cost-efficiency, portable and speedy manner (Gan et al., 2019; Hu and Feng, 2012; Pourreza et al., 2018).

Recently, due to the advantages of convenient operation, low price, and excellent portability, the researchers have made a great deal of efforts to the development of point-of-care testing (POCT) (Cao et al., 2019; Kong et al., 2019a; Zeng et al., 2019). However, some reported POC colorimetric methods using paper as a solid phase carrier for the monitoring of oxalate could only offer the qualitative/semi-quantitative screening, usually suffering from insufficient sensitivity and poor stability in practical applications (Dey et al., 2018; Mahato et al., 2017; Quesada-González and Merkoçi, 2015; Worftamongkona et al., 2018). In order to satisfy the needs for stable and accurate quantitative monitoring, it is urgent to supply some sensors based on other solid-phase carriers to provide effective and simple identification. Stimulus-responsive hydrogels, for example, bio-actuators-responsive hydrogels (Shi et al., 2019), photo-responsive hydrogels (Dong et al., 2018) and multi-responsive hydrogels (Downs et al., 2020), with excellent mechanical stability, biodegradability, and biocompatibility, have attracted more and more attention in the field of encapsulation and immobilization (Caliari and Burdick, 2016; Hao et al., 2017; Vázquez-González and Willner, 2020; Willner, 2017). Hydrogels that offer a relatively inert circumstance in the gel matrix, are regarded as an obstacle to the external environment. On the other hand, the diffusion of substrate molecules is allowed through the porous structure, which ultimately improve the function and stability of the encapsulated material (Ogura and Rehm, 2019a). Thus, hydrogels are considered as one of the most potential solid-phase carriers for oxalate on-site analysis. In addition, smartphone-based detection platforms demonstrated tremendous prospect in on-site applications, due to the widespread coverage of smartphone worldwide. It is reported that numerous smartphone-based platforms can be used in a variety of bioanalytical detection applications, such as colorimetric strategy (Berg et al., 2015; Kong et al., 2019b; Vashist et al., 2015b), fluorometric system (Jin et al., 2019), and microfluidic device (Barbosa et al., 2015). In those applications, the smartphone-based inspection systems performed outstanding performance even compared to bulky and expensive laboratory instruments, which facilitated a variety of POCT applications (Vashist et al. 2014, 2015a).

Enlightened by the aforementioned research, a "lab in a tube" sensing platform integrated with the smartphone was proposed for on-site monitoring of oxalate in a rapid and sensitive manner. Based on the intrinsic oxidase-like catalytic property of manganese dioxide (MnO_2) nanosheets, which could catalyze the oxidation of 3,3′,5,5′-tetramethylbenzidine (TMB) into oxTMB (blue product) (Liu et al., 2017). The stimuli-responsive nanozyme-based hydrogel consisting of the sodium alginate (SA) hydrogel and TMB-MnO_2 nanosheets system were integrated into a commercialized microtube to assemble the portable kit. In the presence of oxalate, MnO_2 nanosheets were reduced to yield Mn^{2+}, further suppressing the color reaction. Thus, the proposed MnO_2-controlled hydrogel kit could be employed to the measurement of oxalate. For accurate quantitative detection, the color changes of portable kit were collected via the smartphone camera. Subsequently, the corresponding image could be converted into hue intensity based on the ImageJ software, which displayed a linear relationship with the concentration of oxalate. It is worth noting that the portable platform was successfully applied to detect the level of oxalate in urine with acceptable results through combining smartphone reader and nanozyme-based hydrogel kit, making the monitoring process convenience and providing a novel way for probing oxalate.

2. Experimental section

2.1. Materials and instruments

All commercially available reagents were purchased in analytical grade and used without further purification. Manganese (II) chloride tetrahydrate ($MnCl_2{\cdot}4H_2O$), sodium hydroxide (NaOH), oxalate, SA, calcium chloride ($CaCl_2$) were purchased from Aladdin Reagent Co. Ltd (Shanghai, China). TMB and dimethylsulfoxide (DMSO) were obtained from Sigma-Aldrich (St. Louis, MO). BSA were purchased from Ryon Biological Technology Co., Ltd. (Shanghai, China). The UV–Vis absorbance measurements were obtained on a UV-2550 spectrometer (Shimadzu). The morphological structures of the samples were found by JEM-2100 transmission electron microscope (TEM).

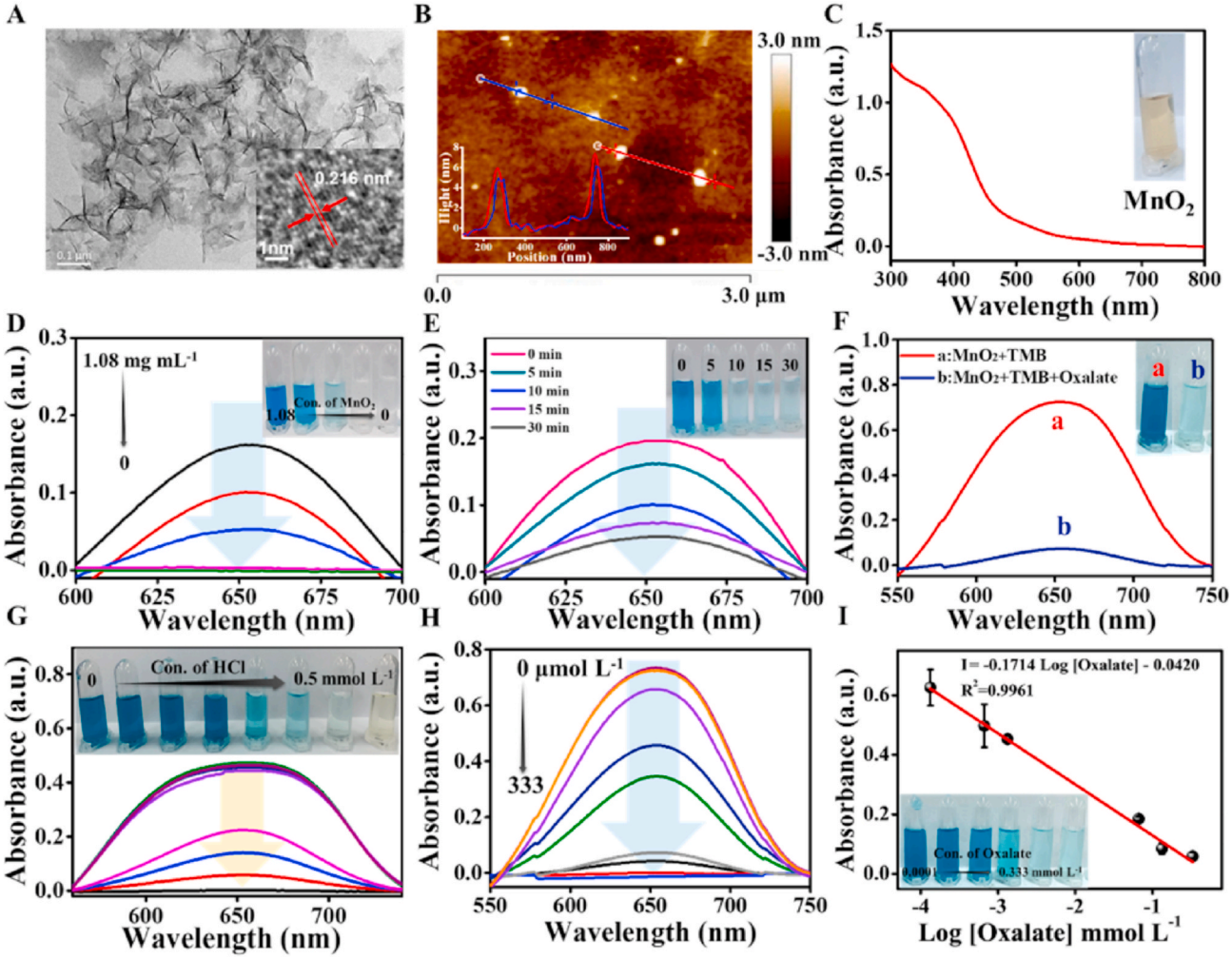

Fig. 1. (A) TEM and HRTEM image of the BSA (0.5 mg mL^{-1})-templated-MnO_2 nanosheets. (B) AFM image and the corresponding height profile of MnO_2 nanosheets. (C) UV–vis absorption spectra of MnO_2 nanosheets (Insert: photograph of MnO_2 nanosheets after storing at room temperature for three weeks). (D) The UV–vis absorption spectra of TMB with different concentrations of MnO_2 nanosheets (1.08, 0.54, 0.36, 0.27, 0 mg mL^{-1}). (E) Effect of the reaction time. (F) UV–vis absorption spectra of TMB-MnO_2 nanosheets system (a), TMB-MnO_2 nanosheets system + oxalate (b). (G) The UV vis absorption spectra of TMB-MnO_2-oxalate system with different concentrations of HCl. (H) UV–vis absorption spectra of MnO_2-TMB system with varying concentrations of oxalate. (I) Linear plot of absorbance intensity ratio versus the concentration of oxalate (Inset: the corresponding photographs of the solution taken under daylight).

2.2. Synthesis of MnO_2 nanosheets hydrogel

Typically, 5.0 mL BSA (0.5 mg mL^{-1}) was mixed with 5.0 mL $MnCl_2{\cdot}4H_2O$ (4.0×10^{-3} mol L^{-1}), the mixture solutions were continuously stirred at room temperature for 1 h. Subsequently, the pH value of the reaction aqueous solution was adjusted to 10 with NaOH (1.0 mol L^{-1}). After reaction for 4 h at 4 °C. Furthermore, SA was sufficiently dissolved in pH 8.0 Tris-HCl buffer, and the SA (20.0 mg mL^{-1}) was quickly transferred into the snap cap of microtube. Then, 0.125 mg mL^{-1} MnO_2 NFs were added into the SA. After thorough mixing, 5.0 mg mL^{-1} $CaCl_2$ solution was added dropwise to the above mixture to make a uniform MnO_2 -SA mixed hydrogel.

2.3. Preparation of the hydrogel kit for oxalate

The measurement was carried out in polypropylene microtubes that was used as a container and reaction platform. The fabrication of stimuli-responsive MnO_2-based hydrogel regarded as a sensing platform for the on-site monitoring of oxalate (Scheme 1). First, the synthesized MnO_2 nanosheets were rooted into sodium alginate, which dropped on a snap cap of microtube, forming hydrogel via introducing Ca^{2+} with an ultra-simple one-step protocol. The hydrogel was regarded as a carrier material with high capacity to absorb and release solutions, and the high stability was suitable for long-term storage of samples (Ogura and Rehm, 2019b). Subsequently, different amounts of oxalate were incubated with 50 μL 100 mmol L^{-1} HCl into the microtube. Then, the microtube turned upside down for 10 min at room temperature to diffuse solution into MnO_2-based hydrogels, causing decomposition of MnO_2 nanosheets to yield Mn^{2+}. To inspect the color change of the MnO_2-hydrogel, the test microtube was turned upside down again and the mixture of 1.5 mmol L^{-1} TMB and acetate buffer (0.1 mol L^{-1}, pH 4.0) was introduced into the snap cap of microtube. Finally, the color information was acquired using a smartphone built-in camera as recorder, which could be analyzed using ImageJ software for quantitative evaluation of oxalate.

2.4. Smartphone-based hydrogel kit analysis

The iron base holder of the hydrogel kit was made with the size of 21.5 × 30.0 × 13.0 cm. The test tube rack was placed in the designated position of the recorder. Subsequently, the colorimetric image was taken by putting the smartphone (Vivo X9) inside the designated smartphone containment on the top of the hood (Fig. S1). The RGB intensity of the acquired images was determined through an image processing algorithm using Image J software. The image processing algorithm was to

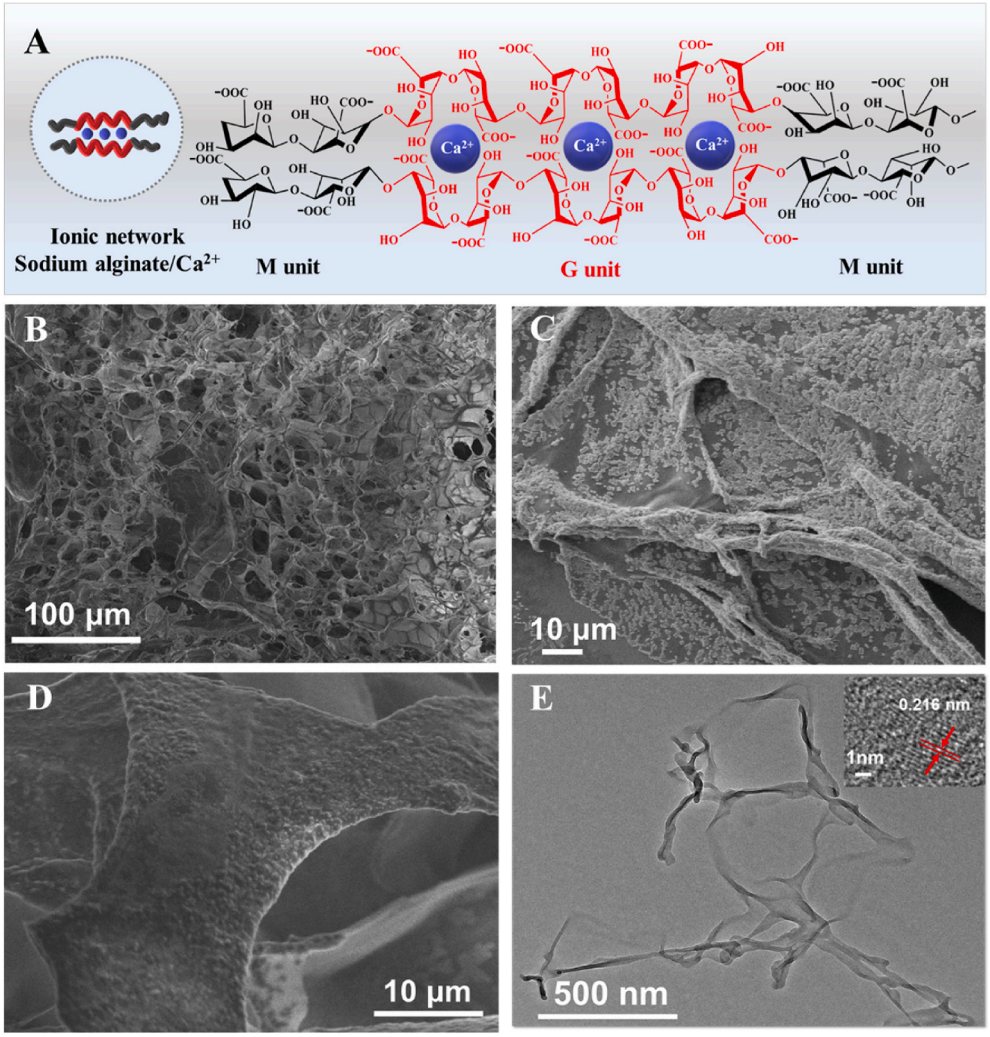

Fig. 2. (A) Chemical structure of G and M monomer and the illustration of chelation by the "egg-box" model in the alginate/Ca^{2+} network. (B) SEM images of SA hydrogels. (C) and (D) SEM images of MnO_2-SA hydrogels. (E) TEM images of freeze-dried MnO_2-SA hydrogels (Insert: HRTEM images of MnO_2-SA hydrogels).

calculate the average intensity of 3 adjacent pixels. Then by standard curve analysis, the calculated required intensity was plotted against the oxalate concentration. The kit images were captured at a fixed distance from the recorder's screen to prevent the parallax error.

2.5. Detection of oxalate in urine sample

Firstly, the human urine sample was diluted 30 times with deionized water and adjusted to pH = 3.0 by adding HCl (100 mmol L^{-1}), then different concentration (8, 80, 800 μmol L^{-1}) of oxalate were prepared using the diluted human urine sample. Next, the reaction solution was turned upside down for 10 min at room temperature. Finally, the mixture of 1.5 mmol L^{-1} TMB and acetate buffer (0.1 mol L^{-1}, pH 4.0) was introduced into the snap cap of microtube. The image of the hydrogel kit was recorded by smartphone and analyzed via the ImageJ software.

3. Results and discussion

3.1. Characterization and the catalytic property of MnO_2 nanosheets

The research was started via the bio-template synthesis of MnO_2 nanosheets, which were nucleated and synthesized with BSA in the alkaline solution (Han et al., 2017). As revealed in Fig. 1A, the MnO_2 nanosheets had a large 2D morphology, indicating that the large surface area of nanostructures increased the probability for the contact with catalytic substrate. The clear lattice fringe with interplanar spacing of 0.216 nm were in consistent with the (420) plane of the MnO_2 (Fig. 1A inset). As clearly displayed in Fig. 1B, the atomic force microscope (AFM) data confirmed that the MnO_2 nanosheets revealed an ultrathin sheet structure with a thickness of approximate 6.0 nm. Furthermore, the UV–vis spectra of MnO_2 nanosheets were manifested a characteristic broadened absorption band within 320 nm–580 nm, which exhibited a characteristic absorption peak at about 380 nm (Fig. 1C). The MnO_2 samples showed a typical brown colloid, which could stabilize for 3 weeks at room temperature without any precipitation (Fig. 1C inset). Taken together, all of these results indicated that the MnO_2 nanosheets were successfully obtained with good stability. To verify the catalytic property, various concentration of MnO_2 were directly incubated with TMB for the colorimetric reaction. As expected, with the decreasing concentration of the MnO_2 nanosheets (0-1.08 mg mL^{-1}), the characteristic absorption peak of the solution decreased gradually as depicted in Fig. 1.. In addition, the solution color changed from blue to colorless (Fig. 1D, inset), which demonstrated the MnO_2 performed oxidase-like activity. Moreover, we found that the absorbance (color) of the solution remained unchanged basically within 5 min, and then decreased significantly, which might be due to the reduction of oxTMB to a certain extent (Fig. 1E). Interestingly, it was known that MnO_2 nanosheets have high reactivity toward oxalate under acidic pH, which could promote the decomposition of MnO_2 nanosheets to form Mn^{2+} (equation (1)),

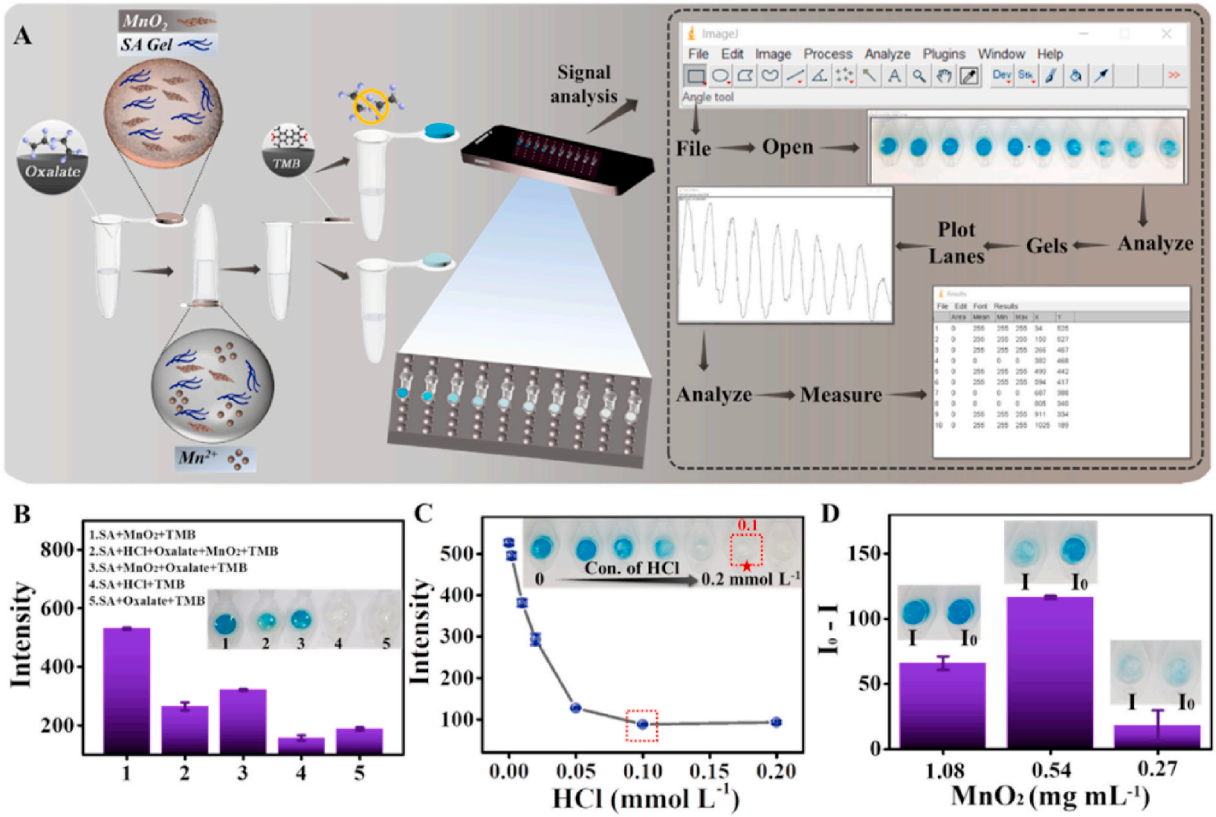

Fig. 3. (A) Reaction process of portable test kit for detection oxalate. (B) Intensity of reaction solution: (1) SA + MnO_2 nanosheets + TMB, (2) SA + HCl + Oxalate + MnO_2 nanosheets + TMB, (3) SA + MnO_2 nanosheets + Oxalate + TMB, (4) SA + HCl + TMB, (5) SA + Oxalate + TMB. (C) The optimization of the concentration of HCl. (D) The optimization of the concentration of MnO_2 nanosheets.

$$MnO_2 + C_2O_4^{-2} + 4H \rightarrow Mn^{2+} + 2CO_2 + 2H_2O \quad (1)$$

the degradation of MnO_2 NFs could be corroborated by the decrease of the characteristic absorption peak of oxTMB at 652 nm (Fig. 1F). The concentration of HCl controlled the pH of the reaction environment, the MnO_2 nanosheets are basically decomposed completely by oxalate when the concentration of HCl was 0.5 mmol L^{-1} (Fig. 1G). In this strategy, the method of oxalate detection was further performed according to the TMB/MnO_2 nanosheets system. Along with the oxalate concentrations increased from 0 to 333 μmol L^{-1}, the absorp$MnO_2 + C_2O_4^{-2} + 4H \rightarrow Mn^{2+} + 2CO_2 + 2H_2O$tion intensity of oxTMB at 652 nm gradually decreased, which corroborated the degradation of MnO_2 nanosheets (Fig. 1H). Meanwhile, the characteristic absorption peak change of system displayed a quality linear fitting (R^2 = 0.9961) with the logarithm of oxalate concentration (Fig. 1I). It was worth noting that the limit of detection (LOD) was as low as 0.1 μmol L^{-1}, which demonstrated that the sensing platform was suitable for oxalate detection. Combined with the above results, the TMB/MnO_2 nanosheets colorimetric system could be considered as an effective and attractive tool for POCT applications.

3.2. Hydrogel-portable kit for accurate detection of oxalate

Based on its simple preparation and favorable biocompatibility, the hydrogel with 3D cross-linked networks structure as a robust carrier could response to physicochemical stimulation, which possessed a broad application prospect in POCT (Cao et al., 2019; Li et al., 2019; Liu et al., 2020). SA as a natural hydrophilic polysaccharide, which was composed of β-D-mannuronic acid (M) unit and α-l-guluronic acid (G) unit connected through β-1, 4 bond (Wang et al., 2019). In the presence of Ca^{2+} (or other divalent cations), G-blocks could be stacked via the formation of "egg-box" calcium linked junctions to obtain hydrogels in an ultra-simple manner (Fig. 2A). Combining with these studies, we constructed a portable kit via immobilizing the MnO_2 nanosheets into SA hydrogel to manufacture TMB-controlled platform for visible detection of oxalate. As illustrated in Fig. 2B, the freeze-dried SA hydrogel was clearly displayed the cross-sectional morphology, revealing a porous layered structure that could load with large amounts of materials. After the introduction of MnO_2 nanosheets, it could be noticed that the protrusions on the gel were MnO_2 two-dimensional structure nanosheets, which was dispersed uniformly and widely on the SA hydrogel (Fig. 2C and D). To further validate the structural information, the SA hydrogels containing MnO_2 nanosheets were characterized with TEM after low temperature vacuum freeze-drying. As shown in Fig. 2E, there were apparent dark streaks on the fibrous hydrogels after introducing MnO_2 nanosheets. At the HRTEM image of hydrogels (Fig. 2E inset), the dark streaks showed clear lattice fringe with interplanar spacing of 0.216 nm identified as MnO_2 nanosheets. Herein, all results demonstrated that MnO_2 nanosheets were successfully encapsulated in the SA hydrogel.

Based on the above results, a stimuli-responsive hydrogel kit with MnO_2 nanosheets probe as the suitable candidate for accurate on-site measurement of oxalate was constructed. As shown in Fig. 3A, MnO_2 nanosheets rooted into SA hydrogels were poured in a snap cap of commercialized microtube via a simple one-step protocol firstly. After introducing the urine containing oxalate into a microtube, it was inverted to let the oxalate diffuse into MnO_2-SA hydrogels. To facilitate observation of the color change of the hydrogel kit, turned the microtube upside down again, and then opened the snap cap. Afterwards, the optical images of the kits obtained through smartphone built-in cameras could be combined with imageJ software to analyze the hue intensity data to quantitatively evaluate the oxalate. In this strategy, MnO_2 nanosheets encapsulated in hydrogel could still directly oxidize TMB to blue product (Figs. 3B and 1). After the introduction of oxalate, the

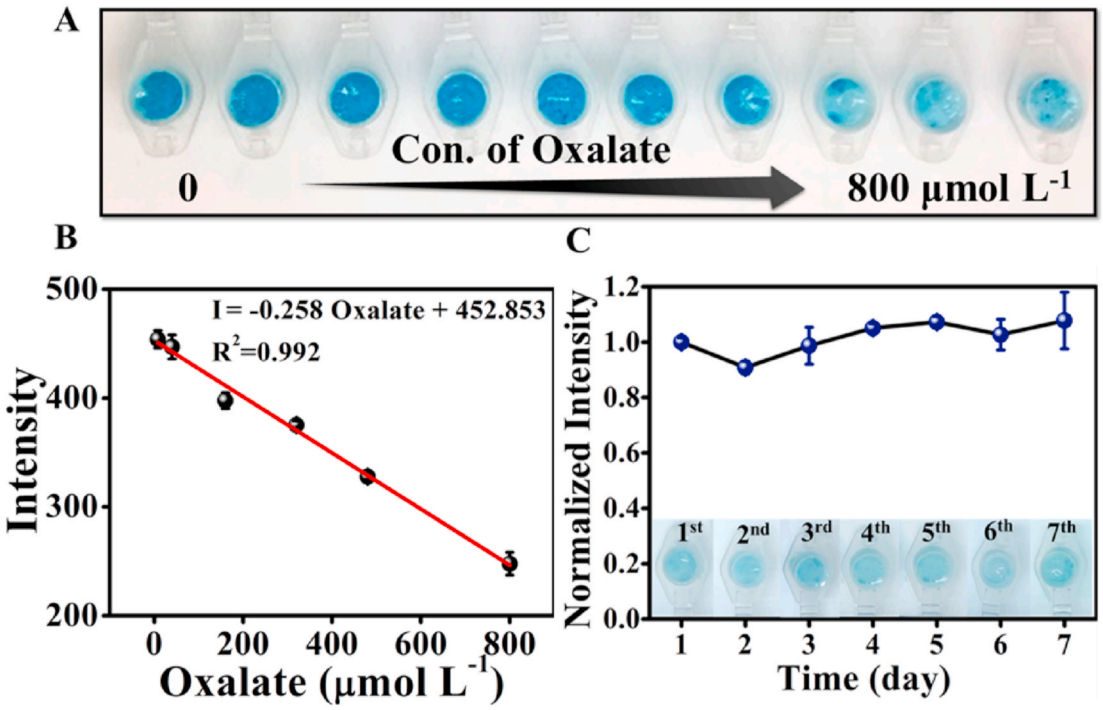

Fig. 4. (A) The photograph of the test kit with different concentrations of oxalate. (B) Relationship between hue intensity and the oxalate concentration. (C) The stability of the kit (with oxalate) within seven days.

decomposition of MnO_2 nanosheets was triggered and the oxidation of TMB was blocked (Fig. 3B and). In addition, the presence of both oxalate and HCl would accelerate the decomposition of MnO_2 nanosheets (Figs. 3B and 2). To validate the system feasibility, oxalate and HCl were introduced into SA-TMB solution separately (Figs. 3B, 4 and 5). There were no significant characteristic color signals in the systems, further confirmed that SA-TMB could not be triggered by those substances. To improve the sensing performance of the hydrogel test kits, some conditions were optimized. As depicted in Fig. 3C, the high concentration of HCl (>0.05 mmol L^{-1}) could contributed to the decomposition of MnO_2 nanosheets, accompanied by significant fade of the hydrogel kit color. The result demonstrated that the C_{HCl} (0.1 mmol L^{-1}) could provide a higher rate of catalytic decomposition. In addition, the concentration of MnO_2 nanosheets was optimized (Fig. 3D), the results revealed that a certain amount of oxalate could decompose the largest amount of 0.54 mg mL^{-1} MnO_2 nanosheets (I_0 - I). In order to maintain the color signal uniform, we have optimized the preparation process of the hydrogel. As shown in Fig. S2, the mixing time of SA and MnO_2 nanosheets was selected 1 min and the mixing time of SA-MnO_2 nanosheets and $CaCl_2$ controlled within 10 s, which could better shield out the color signal nonuniform. Furthermore, compared with dropping 5 μL of $CaCl_2$ (25.0 mg mL^{-1}) on the snap cap of microtube for four times, 20 μL of $CaCl_2$ (25.0 mg mL^{-1}) can better shield out the color signal nonuniform.

Under the optimized conditions, the sensing performance of the MnO_2 nanosheets based hydrogel kit was investigated via introducing oxalate. As illustrated in Fig. 4A, the color of the hydrogel kit changed in a noticeable gradient by increasing the concentration of oxalate from 0 to 800 μmol L^{-1}. Through the image processing technology, the histogram of intensity could be treated as an alternative form of color recognition (Fig. S3), thereby generating a gradient change in the concentration of oxalate (Fig. S4). As shown in Fig. 4B, the converted intensity of hydrogel kits displayed a well linear relationship with the concentration of oxalate in the range from 0.8 to 800 μmol L^{-1} (R^2 = 0.992).

It was worth mentioning that the limit of detection (LOD) was calculated as 0.8 μmol L^{-1}. Moreover, the storage period of sensing platform as a key feature of POC devices was also investigated. In virtue of the protection of the hydrogel, MnO_2 nanosheets lost less than 17% catalytic activity after storing for 7 day at 4 °C (Fig. S5). Moreover, the oxalate-introduced sample showed almost no change within 7 days (Fig. 4C). As revealed in Figs. S6 and S7, the portable kit achieved almost no discoloration for 240 consecutive minutes, which indicated that the kit could maintain a relatively stable state within a certain period of time. The comparison with other oxalate monitoring systems were summarized in Table 1, our proposed hydrogel kit exhibited the unique signal output advantage, which demonstrated a more reliable sensitive performance and the shorter response time (10 min) than other assays. The excellent detection performance of this system derived from amplification technology, which might be attributed to the following unique features: (i) As biomimetic oxidase, the stability of MnO_2 nanosheets performed better than natural enzymes (Liu et al., 2017), which could ameliorate the sensing performance. (ii) The ultrathin-layered MnO_2 nanosheets possessed a typical two-dimensional morphology and exhibited a high specific surface area, which facilitated to provide more catalytic active sites. (iii) As an encapsulating material, SA-hydrogel allowed the substrate molecule to diffuse by the porous structure, while also acting as a barrier to the complex external environment. These results indicated that the integration of MnO_2-based hydrogel kit with smartphone offered a portable platform for accurate monitoring of oxalate.

Specificity ability and anti-interference were significance indicators for assessing the capacity of the constructing hydrogel-based biosensor, especially in POCT application. Thereby, in order to simulate the complex actual environment, other common substances (urea, inorganic salt, amino acid, metal ion and protein) were chosen to evaluate the interference effect of the test kit for oxalate. As revealed in Fig. 5A, the change of normalized intensity histogram manifested that the potential interference substances (10 mmol L^{-1}) could not trigger the decomposition of MnO_2 nanosheets, accompanying the reduction of the intensity signal, while only oxalate (1.0 mmol L^{-1}) induced significant response. The obvious color change of the MnO_2-based hydrogel kit toward oxalate (compared to the blank), while the other control interferences

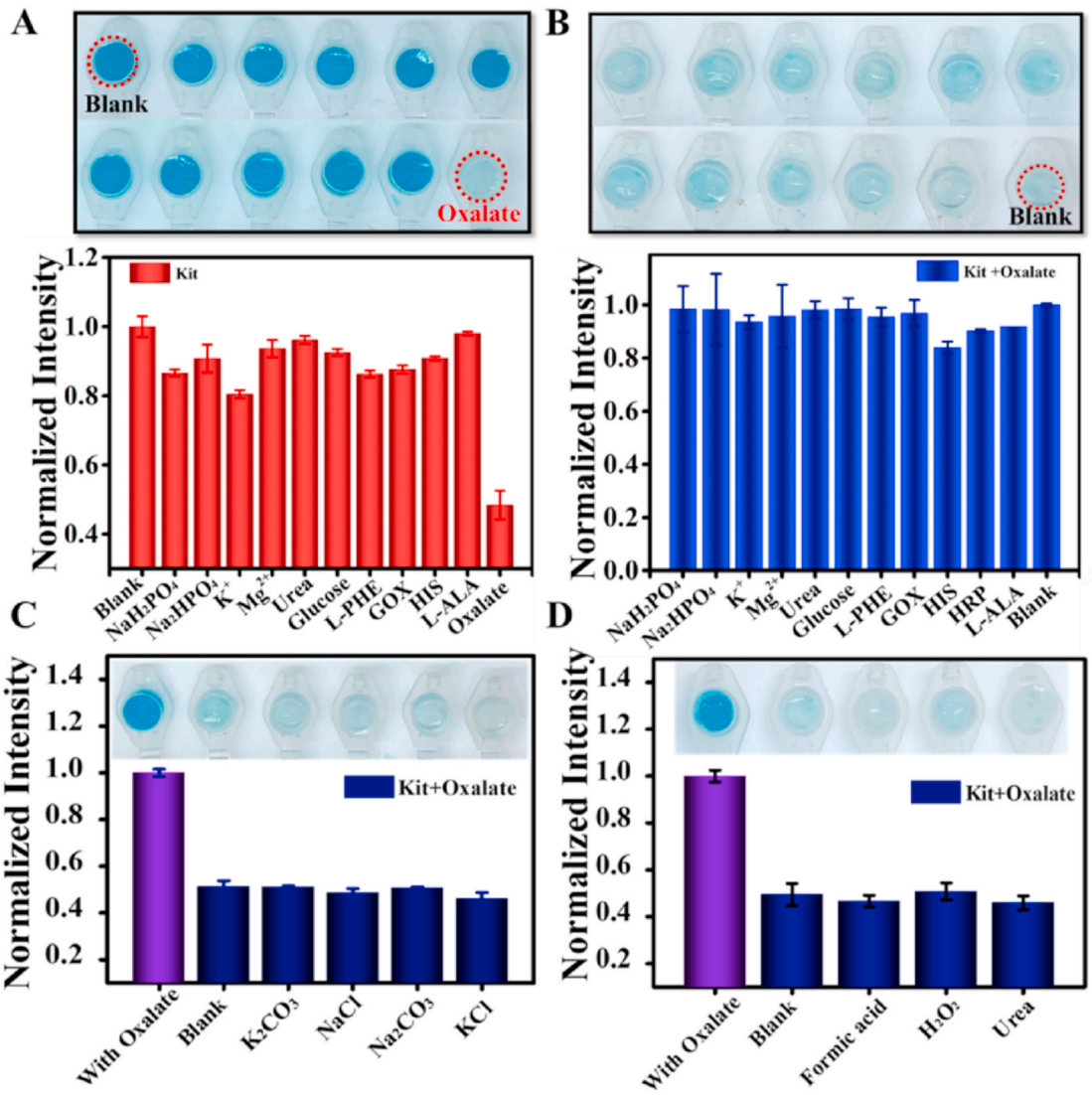

Fig. 5. (A) The selectivity of the hydrogel kit and the photograph in the presence of interfering ions. (B) The anti-interference of the hydrogel kit and the corresponding photograph in the presence of interfering ions. (C) The anti-interference ability of hydrogel kit for inorganic salts (K_2CO_3, NaCl, Na_2CO_3, KCl) in urine (Inset: the corresponding photograph in the presence of interfering inorganic salts). (D) The anti-interference ability of hydrogel kit for formic acid, hydrogen peroxide and urea in urine (Inset: the corresponding photograph in the presence of interfering these potential redox substances).

Table 1
Comparison of performance of different oxalate probing strategy.

Method	LOD (μmol L^{-1})	Response time	Portability	Reference
Paper-based colorimetric device	10	30 min	Yes	Worftamongkona et al. (2018)
TiO_2 nanoparticles/ multiwalled carbon nanotubes modified electrode	33	>30 min	No	Fakhari et al. (2012)
Carbon ionic liquid electrode modified with TiO_2–Fe nanoparticles	23	>15 min	No	Akhond et al. (2016)
Amperometric biosensor	1	7s	No	Pundir et al. (2011)
Smartphone-portable hydrogel kit	0.8	10 min	Yes	This work

substances did not occur, indicating strong a selectivity ability of kit. Following, the signals of the above co-existing substances with oxalate were almost the same, demonstrating the hydrogel kit performed strong anti-interference ability. In addition, the color change represented that in the presence of co-existing substances, the response of the hydrogel kit toward oxalate remained constant. (Fig. 5B). The effect of some potential redox substances including formic acid and hydrogen peroxide and other co-existing substances (urea, K_2CO_3, NaCl, Na_2CO_3 and KCl) in urine were evaluated as shown in Fig. 5C and D. The change of normalized intensity histogram represented that in the presence of co-existing substances, the response of the hydrogel kit toward oxalate remained constant. Taken together, the MnO_2-based hydrogel system exhibited high specificity and anti-interference performance for the monitoring of oxalate.

3.3. Detection of oxalate in urine sample

From a practical point of view, the excessively high concentration of oxalate in the urine (>300 μ) evidenced the risk of diseases such as urolithiasis, so the monitoring of oxalate in the actual sample was of great significance. In this work, human urine was selected as model

Table 2
Spiked real sample analysis using the smartphone-based hydrogel kit.

Sample	Added (μmol L^{-1})	Found (μmol L^{-1})	Recovery (n = 3, %)	RSD (n = 3, %)
Urine	8	8.28	103.60	8.50
	80	78.96	98.69	4.16
	800	807.20	100.94	8.54

matrix for investigating the potential POCT application of the proposed platform. Subsequently, the accuracy of the hydrogel kit in practice application was evaluated via measuring the recovery based on the standard addition method. As illustrated in Table 2, the recovery rates of the samples were in the range of 98.69–103.60% with the relative standard deviations (RSDs) from 4.16% to 8.54%, indicating the capability of the protable kit for quantitative analysis of oxalate in human urine. Evidently, due to the merits of the facile usage and superior stability of hydrogel, the good operability and high efficiency of the portable kit provided a potential prospect for quantitative POC screening of oxalate for ensuring food safety and estimating poisoning.

4. Conclusions

In summary, the all-in-one platform combined a stimuli-responsive hydrogel as a cost-effective encapsulated material with high loading capacity and a kit as a portable, simple setup for on-site analysis of oxalate. Compared with the traditional analysis methodology, this portable hydrogel biosensor used stimuli-responsive hydrogels as encapsulating materials, allowing substrate molecules to diffuse through the porous structure to improve sensing efficiency. Moreover, ultrathin two-dimensional MnO_2 nanosheets were synthesized via a simple biotemplate approach. In view of its large specific surface area and high oxidase-like activity, it could be utilized as an enhanced signal label. As the most brilliant part, this platform was capable of screening twelve samples within 10 min for high-throughput analysis in a sensitive method, without the need for washing steps. In general, owing to its accuracy and rapidity, the smartphone hydrogel-portable platform offered a novel sight for quantitative on-site analysis of oxalate to ensure food safety and disease prevention.

CRediT authorship contribution statement

Rui Jin: Conceptualization, Methodology, Writing - original draft. **Lianjing Zhao:** Conceptualization. **Xu Yan:** Conceptualization, Methodology, Funding acquisition, Supervision. **Xiaosong Han:** Methodology, Writing - original draft. **Mengqi Liu:** Writing - original draft. **Yue Chen:** Writing - original draft. **Dandan Su:** Methodology, Writing - original draft. **Fangmeng Liu:** Methodology. **Peng Sun:** Methodology, Supervision. **Xiaomin Liu:** Writing - original draft. **Chenguang Wang:** Supervision. **Geyu Lu:** Funding acquisition, Supervision.

Declaration of competing interest

The authors declare that they have no known competing financial interests or personal relationships that could have appeared to influence the work reported in this paper.

Acknowledgements

This work was supported by the National Nature Science Foundation of China (Grant Numbers 21806051, 61831011, 61722305, 61875191 and 61833006). China Postdoctoral Science Foundation funded project (No. 2020M670857). Natural Science Foundation of Jilin Province (20200201021JC and 20200201218JC). Scientific and Technological "13th Five-Year Plan" Project of Jilin Provincial Department of Education (NO. JJKH20190111KJ and JJKH20201010KJ). The National Key Research and Development Program of China (Grant Numbers 2016YFC0207300). Program for JLU Science and Technology Innovative Research Team (JLUSTIRT 2017TD-07). The Graduate Innovation Fund of Jilin University (Grant Numbers 101832018C016).

Appendix A. Supplementary data

Supplementary data to this article can be found online at https://doi.org/10.1016/j.bios.2020.112457.

References

Akhond, M., Absalan, G., Tafakori, A., Ershadifar, H., 2016. Anal. Bioanal. Chem. Res. 3, 73–86.
Barbosa, A.I., Gehlot, P., Sidapra, K., Edwards, A.D., Reis, N.M., 2015. Biosens. Bioelectron. 70, 5–14.
Berg, B., Cortazar, B., Tseng, D., Ozkan, H., Feng, S., Wei, Q., Chan, R.Y.-L., Burbano, J., Farooqui, Q., Lewinski, M., Di Carlo, D., Garner, O.B., Ozcan, A., 2015. ACS Nano 9, 7857–7866.
Caliari, S.R., Burdick, J.A., 2016. Nat. Methods 13, 405–414.
Cao, H., Wang, Y., Gao, Y., Deng, X., Cong, Y., Liu, Y., Jiang, X., 2019. Angew. Chem. Int. Ed. 58, 1626–1631.
del Nozal, M.J., Bernal, J.L., Diego, J.C., Gómez, L.A., Ruiz, J.M., Higes, M., 2000. J. Chromatogr. A 881, 629–638.
Dey, N., Kumari, N., Bhagat, D., Bhattacharya, S., 2018. Tetrahedron 74, 4457–4465.
Dong, Y., Jin, G., Hong, Y., Zhu, H., Lu, T.J., Xu, F., Bai, D., Lin, M., 2018. ACS Appl. Mater. Interfaces 10, 12374–12389.
Downs, F.G., Lunn, D.J., Booth, M.J., Sauer, J.B., Ramsay, W.J., Klemperer, R.G., Hawker, C.J., Bayley, H., 2020. Nat. Chem. 12, 363–371.
Fakhari, A.R., Rafiee, B., Ahmar, H., Bagheri, A., 2012. Anal. Methods 4, 3314–3319.
Gan, Y., Hua, N., He, C., Zhou, S., Tu, J., Liang, T., Pan, Y., Kirsanov, D., Legin, A., Wan, H., Wang, P., 2019. Biosens. Bioelectron. 130, 254–261.
Han, L., Liu, P., Zhang, H., Li, F., Liu, A., 2017. Chem. Commun. 53, 5216–5219.
Hao, T., Li, J., Yao, F., Dong, D., Wang, Y., Yang, B., Wang, C., 2017. ACS Nano 11, 5474–5488.
He, K., Li, Z., Wang, L., Fu, Y., Quan, H., Li, Y., Wang, X., Gunasekaran, S., Xu, X., 2019. ACS Appl. Mater. Interfaces 11, 26250–26260.
Hong, F., Nilvebrant, N.-O., Jönsson, L.J., 2003. Biosens. Bioelectron. 18, 1173–1181.
Hu, M., Feng, G., 2012. Chem. Commun. 48, 6951–6953.
Jin, R., Kong, D., Yan, X., Zhao, X., Li, H., Liu, F., Sun, P., Lin, Y., Lu, G., 2019. ACS Appl. Mater. Interfaces 11, 27605–27614.
Kong, D., Jin, R., Wang, T., Li, H., Yan, X., Su, D., Wang, C., Liu, F., Sun, P., Liu, X., Gao, Y., Ma, J., Liang, X., Lu, G., 2019a. Biosens. Bioelectron. 145, 111706.
Kong, D., Jin, R., Zhao, X., Li, H., Yan, X., Liu, F., Sun, P., Gao, Y., Liang, X., Lin, Y., Lu, G., 2019b. ACS Appl. Mater. Interfaces 11, 11857–11864.
Li, H., Chai, X.-S., DeMartini, N., Zhan, H., Fu, S., 2008. J. Chromatogr. A 1192, 208–211.
Li, Y., Ma, Y., Jiao, X., Li, T., Lv, Z., Yang, C.J., Zhang, X., Wen, Y., 2019. Nat. Commun. 10, 1036.
Liu, D., Wang, J., Wu, L., Huang, Y., Zhang, Y., Zhu, M., Wang, Y., Zhu, Z., Yang, C., 2020. TrAC Trends Anal. Chem. (Reference Ed.) 122, 115701.
Liu, J., Meng, L., Fei, Z., Dyson, P.J., Jing, X., Liu, X., 2017. Biosens. Bioelectron. 90, 69–74.
Mahato, K., Srivastava, A., Chandra, P., 2017. Biosens. Bioelectron. 96, 246–259.
Maya, F., Estela, J.M., Cerdà, V., 2011. Microchim. Acta 173, 33–41.
Mercey, G., Verdelet, T., Renou, J., Kliachyna, M., Baati, R., Nachon, F., Jean, L., Renard, P.-Y., 2012. Accounts Chem. Res. 45, 756–766.
Ogura, K., Rehm, B.H.A., 2019a. Adv. Funct. Mater. 29, 1901893.
Ogura, K., Rehm, B.H.A., 2019b. Adv. Funct. Mater. 29.
Pourreza, N., Lotfizadeh, N., Golmohammadi, H., 2018. Spectrochim. Acta 192, 251–256.
Pundir, C.S., Chauhan, N., Rajneesh, Verma, M., Ravi, 2011. Sensor. Actuator. B Chem. 155, 796–803.
Quesada-González, D., Merkoçi, A., 2015. Biosens. Bioelectron. 73, 47–63.
Shi, Q., Liu, H., Tang, D., Li, Y., Li, X., Xu, F., 2019. NPG Asia Mater. 11, 64.
Uniyal, S., Sharma, R.K., 2018. Biosens. Bioelectron. 116, 37–50.
Vashist, S.K., Luppa, P.B., Yeo, L.Y., Ozcan, A., Luong, J.H.T., 2015a. Trends Biotechnol. 33, 692–705.
Vashist, S.K., Mudanyali, O., Schneider, E.M., Zengerle, R., Ozcan, A., 2014. Anal. Bioanal. Chem. 406, 3263–3277.
Vashist, S.K., van Oordt, T., Schneider, E.M., Zengerle, R., von Stetten, F., Luong, J.H.T., 2015b. Biosens. Bioelectron. 67, 248–255.
Vázquez-González, M., Willner, I., 2020. Angew. Chem. Int. Ed. 59, 2–38.
Wang, L., Zhang, X., Xia, Y., Zhao, X., Xue, Z., Sui, K., Dong, X., Wang, D., 2019. Adv. Mater. 31, 1902381.
Willner, I., 2017. Accounts Chem. Res. 50, 657–658.

Worftamongkona, P., Seeda, K., Phansomboon, P., Ratnarathorn, N., Chailapakul, O., Dungghai, W., 2018. Anal. Sci. 34, 103–108.
Yan, X., Li, H., Su, X., 2018. TrAC Trends Anal. Chem. (Reference Ed.) 103, 1–20.
Zeng, F., Duan, W., Zhu, B., Mu, T., Zhu, L., Guo, J., Ma, X., 2019. Anal. Chem. 91, 1064–1070.
Zhai, Q.-Z., Zhang, X.-X., Liu, Q.-Z., 2006. Spectrochim. Acta 65, 1–4.